Model of single bubble sonoluminescence

Yu An
Department of Physics, Tsinghua University, Beijing 100084

C. F. Ying
Institute of Acoustics, Chinese Academy of Science, Beijing 100080
(Received 14 August 2004; published 21 March 2005)

The temperature within and the sonoluminescence characteristics of a stable inert-gas single bubble grown in water under some given conditions are computed by using a model that is as sufficiently complete as we can manage, except that possible chemical reactions within the bubble are neglected. We work with several different versions of the equation describing the motion of the bubble wall, which are usually considered to give merely slight differences; or vary a parameter in the formula calculating the net increment of the water condensed at the bubble wall. It is found that the final outcomes of the temperature and the sonoluminescence can be significantly different in some cases. This illustration points to the importance of differentiating among the various seemingly similar equations and of adopting the correct value of the parameter used in the computation model of a single bubble.

DOI: 10.1103/PhysRevE.71.036308 PACS number(s): 78.60.Mq, 51.20.+d, 52.35.Tc, 64.70.Fx

I. INTRODUCTION

A single oscillating gas bubble can be trapped at the velocity node of an acoustic standing wave in water. A fascinating accompanying phenomenon is the periodic emission of picosecond light pulses by the bubble in synchronization with oscillation of the acoustic field, which is known as single bubble sonoluminescence or simply SBSL. [1,2]. For SBSL, it is generally understood that the light flash results from the high temperature (hot spot) produced inside the bubble during the bubble compression. It is also usually believed that the high temperature weakly ionizes the interior gas and the stripped electrons lose energy to the photon field to emit light. Of the various possible electron-photon couplings, the bremsstrahlung (electron-ion and electron–neutral-atom) and the recombination of electrons and ions are considered to be the dominant processes [3–5]. Recently, the concept of weak ionization has been doubted [6].

When considering theoretical evaluation of the physical state inside the single bubble as well as the characteristics of the emitted light flash, complicated conditions are confronted and careful modeling is requisite accordingly, even for a simple single bubble (SB) containing an inert gas and grown in pure water which is the object to be studied in this paper. In modeling, all important physical content (or "phenomena") should be included, content such as the liquid compressibility, the diffusion between the gas and the vapor, any possible chemical reactions in the gas and the vapor, and other items. Through some overdue development of modeling, the last ten years have witnessed some drastic changes in the predicted outcomes in the field of SBSL, in particular the temperature inside the bubble.

In this paper, we shall not address the significance of inclusion of relevant important physical content, but aim to study the effects of choice of the physical equations and physical parameters used for the description of these contents. For the sake of simplicity, we hereinafter shall call these equations and parameters the physical "elements" of a model. An "element" can have a number of varieties (or versions), which differ to some extent but relate to the same phenomenon. Varieties exist either because they are equivalent within known limits or because it is uncertain which one is the most exact.

An example of an element is the equations used for the description of the gas motion inside a SB. In quite a few earlier papers, the temperature and density of the gas in the bubble were assumed to be spatially uniform [4,5,7]. The motion of the gas in the bubble was then formulated accordingly. In this narrow sense, the model is called the uniform model. On the other hand, the description of the gas motion in the bubble in terms of the partial differential equations (PDEs) of fluid mechanics was developed by others. Here the phenomenon of gas motion is the same but the element is varied.

An obvious consequence of the choice of different varieties of an element is the generally different theoretical predictions of the physical quantity under study. Usually one variety of the element appears for some reason to be more reasonable than the other. Then the theoretical prediction on the basis of the former variety can be claimed to be more correct. Yet experimental comparison sometimes gives a contrary indication, hence some explanation has to be found.

Return to the uniform model and the PDE model. In spite of its simplicity, the uniform model did succeed in interpreting [4,5,7] some of the experimentally observed characteristics of the SBSL while the PDE model in one case gave a maximum temperature in the interior gas [8] too low to support the bremsstrahlung mechanism (some details will be provided later). This could cast doubt on the validity of the mechanism.

On the basis of the concept of model element, nevertheless we suggest an alternative or supplementary point of view. In a model for a SB, there usually are a various physical "contents" each with its associated "element," which may have more than one variety. In modeling, the most proper element variety has not always been selected for every phe-

nomenon, nor will every element affect the final theoretical outcome significantly. The trouble is it is often unknown which element or elements are sufficiently potent.

The present paper intends to study the effects of changing the varieties of a very small portion of elements in the computation of the temperature inside a SB and the characteristics of its light emission. The bubble is grown in water and contains an inert gas and water vapor. In modeling, all the important physical content will be taken into account except, for simplicity, for the phenomenon of chemical reactions in the interior of the bubble. This omission forbids the direct comparison of our results with any experimental observation but permits some indirect comparison. The important physical content includes the motion of the bubble wall, the water evaporation and the vapor condensation at the bubble wall, the gas motion inside the bubble, the heat exchange at the gas-liquid interface, and the gas ionization and light emission on bubble compression. For all except the first two, we shall adopt fixed elements, which are assumed by us to be proper or satisfactory. For the first two items, on the contrary, we select some varieties of the corresponding elements and compute to see the effects of these variations.

The first element involves the so-called modified Rayleigh-Plesset (RP) [9] equations, while the second involves a formula that governs the condensation and evaporation of water at the bubble wall and contains a parameter to be varied. We shall also make comparison of bubbles containing three different inert gases He, Ar, and Xe, respectively.

This paper is organized as follows. The detailed description of the calculation model is provided in the next section; then, the temperature within and the sonoluminescence characteristics of a single bubble are calculated by varying the equation of radial motion of the bubble wall, viz., the modified RP equation, and the accommodation coefficient of water vapor; a summary and discussion are presented in the final section.

II. COMPUTATION MODEL

As usual, the single bubble under discussion is trapped in water and under the action of an acoustical wave. It is assumed to be spherical all the time. The bubble wall can thus be described by an equation governing its radial motion. Two gas species, the inert gas and water vapor, fill the bubble. Water evaporation from the bubble wall and vapor condensation onto the bubble wall will be considered but mass transport of the inert gas across the wall will be neglected [10]. For the sake of simplicity, the chemical reactions inside the bubble will be ignored; this is permissible as long as it is not our aim to procure exact solutions for experimental comparison. The ambient temperature of the water has several constant values. Under such circumstances, we shall compute some bubble characteristics including the temperature and the pressure inside the bubble as functions of time and space as well as the emitted light intensity, the light spectrum, and the light pulse form.

The computation model for such a SB consists of the following elements: the equation of radial motion of the bubble wall, the formula of water evaporation and vapor condensation at the bubble wall, the gas dynamics equations, the energy equation in liquid for exterior temperature evaluation, and the bremsstrahlung formulas for SBSL. Below, we shall fix the last three model elements but leave the first two slightly varying to examine the consequences of such variation. The second model element will be varied only by dint of varying one of the parameters, which is the accommodation coefficient of water vapor.

A. Equation of radial motion of a spherical bubble

The earlier form of this equation is the classical RP equation [9] that applies to the case of bubble oscillating in an incompressible liquid. For the bubble in a compressible liquid, it is derived from several different forms of the equation, for example, the Gilmore formulation [11], and the Prosperetti-Lezzi formulation [12], and the Keller-Miksis formulation [13]. The last formula can be expressed as

$$(1-M)R\ddot{R}+\frac{3}{2}\left(1-\frac{M}{3}\right)\dot{R}^2=(1+M)\frac{1}{\rho_{l\infty}}[p_l-p_\infty-p_s(t+t_R)]+\frac{t_R}{\rho_{l\infty}}\dot{p}_l, \tag{1}$$

where $R(t)$ is the radius of the bubble, $\rho_{l\infty}$ the ambient liquid density, p_∞ the ambient pressure, $p_s(t)=-p_a\sin(\omega t)$ the driving acoustic pressure, $t_R\equiv R/c_{l\infty}$, $c_{l\infty}$ the sound speed in the liquid at the ambient temperature and pressure of 1 atm, $p_l=p_g(R,t)-4\eta\dot{R}/R-2\sigma/R$, the pressure on the liquid side of the bubble wall, $p_g(R,t)$ the pressure on the gas side of the bubble wall, η the dynamic viscosity, and σ the surface tension coefficient of the liquid. The parameter $M\equiv\dot{R}/c_{l\infty}$ is the bubble-wall Mach number which in fact embodies the effect of the liquid compressibility. The Keller-Miksis formula, along with the other formulas mentioned above and some more which are valid for compressible liquids, are all derived under the condition that $M\ll 1$. In other words, these equations are accurate to the first order in M. When $M\to 0$, all these equations approach the classical RP equation and hence we shall call them the modified RP equations. It is to be emphasized that the sonoluminescence is produced when the bubble is violently compressed, at which time $M\sim 1$. Those modified RP equations with $M\ll 1$ are therefore invalid in a rigorous sense in the real situation of SBSL. To improve the situation somewhat, one may replace $c_{l\infty}$ in Eq. (1) by c_l, where c_l is the sound speed on the liquid side of the bubble wall, which increases with the liquid pressure and consequently will diminish the value of M, which is now R/c_l. One may also simultaneously replace in Eq. (1) $\rho_{l\infty}$ by ρ_l, where ρ_l is the liquid density on the liquid side of the bubble wall. The significance of using new c_l and ρ_l in Eq. (1) may be understood as follows. In this equation (and also in the classical RP equation) the term $(t_R/\rho_{l\infty})\dot{p}_l$ represents a correction for the bubble acoustic radiation. This term may be more precisely written as $(R/c_l)\dot{H}_l$, where $H_l\equiv\int_{p_\infty}^{p_l}dp/\rho_l$ is the enthalpy of the liquid [11,12]. Using the Tait equation, which is an equation of state of water,

$$\frac{p_l + B}{p_\infty + B} = \left(\frac{\rho_l}{\rho_{l\infty}}\right)^n, \tag{2}$$

where B and n are constants, which slightly depend on temperature and are taken to be $B=3638.17$ bar and $n=6.015$ throughout the following calculation, it is easy to show that $(R/c_l)\dot{H}_l=(R/c_l\rho_l)\dot{p}_l$, which is just the term $(t_R/\rho_{l\infty})\dot{p}_l$ in Eq. (1) with $\rho_{l\infty}$ and $c_{l\infty}$ replaced by ρ_l and c_l, respectively. It is uncertain at present whether and how much these replacements will help; we shall study their effects below. ρ_l and c_l are determined as follows: ρ_l is to be computed from the Tait equation (2), and c_l is then evaluated as

$$c_l = \sqrt{\frac{n(p_l + B)}{\rho_l}}.$$

For convenience of description, we shall name the equations formed from different choices of M, ρ, and c in Eq. (1) as follows, where MRP stands for modified RP equation: MRP1 is the Keller-Miksis equation (1), MRP2 is the classical RP equation, which is Eq. (1), with $M=0$, MRP3 is Eq. (1) with $\rho_{l\infty}$ and $c_{l\infty}$ replaced by ρ_l and c_l, respectively, and, MRP4 is the classical RP equation with $c_{l\infty}$ and $\rho_{l\infty}$ replaced by c_l and ρ_l, respectively.

B. Formula of water evaporation and vapor condensation and the accommodation coefficient of water vapor

When a bubble is expanding, the surrounding water evaporates into the bubble; when the bubble is being compressed, the water vapor condenses onto the bubble wall. During the phase transformation, the rate of net mass increment of the condensed vapor (or of the evaporated water for negative sign) at the bubble wall is evaluated by following formula [14]:

$$\dot{m} = \left(\frac{M_1}{2\pi k}\right)^{1/2} \alpha \left.\frac{\Gamma p_1 - p_v}{\sqrt{T_R}}\right|_{r=R}, \tag{3}$$

where M_1 is the mass of a vapor molecule, k the Boltzmann constant, p_1 the partial pressure of the vapor on the gas side of the bubble wall, p_v the saturated vapor pressure at the temperature of the interface T_R. Γ is a correction for bulk motion to the interface, $\Gamma(a)=\exp(-a^2)+a\sqrt{\pi}[1+\mathrm{erf}(a)]$, where $a=(\dot{m}/\rho_1)\sqrt{M_1/2kT_R}$ and ρ_1 is the vapor density on the gas side of the bubble wall. When the temperature (or pressure) at the interface exceeds the critical temperature (or pressure) of water, the formula (3) ceases to be valid. During this period of time, an approximation will be taken as in Ref. [8] in which the evaporation and condensation is assumed to halt.

Now pay attention to the parameter α in the formula (3). This parameter is known as the accommodation coefficient of water vapor. The value of α is not very certain for water. In the common case, it has been taken as 0.03 approximately [14], but it is often taken to be 0.4 for SBSL calculation [8,15]. In the present paper, it will be made adjustable.

Of the many model elements in our computation model, the above two, viz., the modified RP equations and the accommodation coefficient of water vapor, are those that will be varied in order to expose their influences on predicting the temperature and the sonoluminescence. Several other elements exist which will be listed below, but they will not be examined for their effects of variation and henceforth will be fixed.

C. Gas dynamic equations

In the case of SBSL, only the inert gases and the vapor of surrounding liquid can fill the bubble due to the effect of the inert gas rectification [16]. In the present model, two gas species, the inert gas and the water vapor, are assumed to be within the bubble. The partial differential equations of fluid mechanics of two kinds of gas component in spherical symmetry take the following form:

$$\frac{\partial \rho_1}{\partial t} + \frac{1}{r^2}\frac{\partial}{\partial r}[r^2(\rho_1 v + J_1)] = 0,$$

$$\frac{\partial \rho}{\partial t} + \frac{1}{r^2}\frac{\partial}{\partial r}(r^2\rho v) = 0,$$

$$\frac{\partial(\rho v)}{\partial t} + \frac{1}{r^2}\frac{\partial}{\partial r}(r^2\rho v^2) + \frac{\partial p}{\partial r} = \frac{1}{r^2}\frac{\partial}{\partial r}(r^2\tau_{rr}) + \frac{\tau_{rr}}{r},$$

$$\frac{\partial E}{\partial t} + \frac{1}{r^2}\frac{\partial}{\partial r}\{r^2[(E+p)v + q]\} = \frac{1}{r^2}\frac{\partial}{\partial r}(r^2 v\,\tau_{rr}), \tag{4}$$

where t is the time, r the radial coordinate, ρ_i the density of the ith gas, $\rho=\rho_1+\rho_2$ the density of the gas mixture, v_i the radial component of the ith gas velocity, v the average velocity, $\rho v=\rho_1 v_1+\rho_2 v_2$, p the gas pressure, q the heat flux, J_1 the diffusion mass flux of species 1 (the vapor) with respect to the average velocity, $J_1=\rho_1(v_1-v)$, $\tau_{rr}=(4\mu/3)(\partial v/\partial r - v/r)$, μ is the dynamic viscosity, $E=E_1+E_2$ the total energy density, $E_i=\frac{1}{2}\rho_i v_i^2+\rho_i e_i$, and e_i is the internal energy of the ith gas. If one rewrites the total energy density of the gas mixture as $E=\frac{1}{2}\rho v^2+S$, then

$$S = \frac{1}{2}\left(\frac{1}{\rho_1}+\frac{1}{\rho_2}\right)J_1^2 + \left[\frac{3}{2}\nu_2 + \nu_1\left(3 + \sum_{i=1}^{3}\frac{\theta_i/T}{\exp(\theta_i/T)-1}\right)\right]\tilde{R}T, \tag{5}$$

where ν_1 and ν_2 are the mole density of the vapor and the inert gas, respectively, $\tilde{R}=8.31$ J/mol K the gas constant, T the temperature, and θ_i are three vibration energies of the water molecule, $\theta_1=5160$ K, $\theta_2=5360$ K, and $\theta_3=2290$ K. Some detailed formulas calculating the diffusion mass flux, the heat flux, and the viscosity are sketched in Appendix A.

The equation of state of the gases inside the bubble takes the van der Waals form

$$p = \frac{\nu\tilde{R}T}{1-\nu b} - \nu^2 a, \tag{6}$$

where $\nu=\nu_1+\nu_2$ is the mole density of the gas mixture, and a and b are the parameters of the van der Waals equation. For the formulas calculating the parameters a and b, see Appendix B.

Mass conservation requires the following condition at the bubble wall: $(\rho/\rho_2)\, J_1|_{r=R}=\dot{m}$. The other boundary conditions are, at the center of the bubble, $v_i|_{r=0}=0$, $q|_{r=0}=0$, $(\partial\rho_i/\partial r)|_{r=0}=0$; at the bubble wall $v|_{r=R}=\dot{R}+\dot{m}/\rho|_{r=R}$.

In the present model, chemical reactions are not under consideration, and the energy loss due to molecular dissociation is excluded. However, the vibration energy wastage may partly compensate for the energy loss due to the chemical reactions. The reason is as follows: when chemical dissociation occurs, which is usually endothermal, the molecule is dissociated and the energy wastage due to the corresponding molecular vibration no longer needs to be taken into account; whereas in the present model, no dissociation takes place and the energy wastage due to the molecular vibration has to be taken into account all the time.

D. Energy equation in liquid

To evaluate the heat exchange at the interface, the temperature changes in the water should be calculated. With the reference to the work of Voung and Szeri [17], the temperature of the water can be computed by the energy conservative equation

$$\frac{\partial T_l}{\partial t}+v_l\frac{\partial T_l}{\partial r}=D_l\frac{1}{r^2}\frac{\partial}{\partial r}\left(r^2\frac{\partial T_l}{\partial r}\right), \tag{7}$$

where T_l is the temperature (it is identical to the gas temperature at the bubble wall), v_l the velocity of water, approximately $v_l=R^2\dot{R}/r^2$, $D_l=\lambda_l/\rho_l c_{p,l}$ the thermal diffusion coefficient, and λ_l the thermal conductivity of water, which is a function of the temperature [18],

$$\lambda_l(T_l)=-0.3838+5.254\times10^{-3}T_l-6.369\times10^{-6}T_l^2,\quad T_l<T_{c1}, \tag{8}$$

where T_{c1} is the critical temperature of water, for $T_l>T_{c1}$ simply $\lambda_l=\lambda_l(T_{c1})$, and $c_{p,l}$ is the specific heat of water, which is simply assumed to be constant $c_{p,l}=c_{p,l\infty}$, as is the density $\rho_l=\rho_{l\infty}$. Because the heat capacity of water is large compared to that of the gas in the bubble, the temperature changes of the water are mainly limited to the near vicinity of the bubble wall. For this reason, the region outside the bubble is partitioned into two parts, the thin layer and the rest. The thickness of this layer is set as $\Delta=0.1$ μm. Equation (7) holds in the thin layer while the following transformed equation is applied to the remainder:

$$\frac{\partial T_l}{\partial t}=-\frac{2\dot{R}}{R_1}(1-z)\ln(1-z)\frac{\partial T_l}{\partial z}+\frac{(1-z)D_l}{R_z^2}\frac{\partial}{\partial z}\times\left[\left(1-3\frac{R_z}{R_1}\ln(1-z)\right)^{4/3}(1-z)\frac{\partial T_l}{\partial z}\right], \tag{9}$$

where the new variable z, as in [19], is defined by $(r^3-R_1^3)/3=-R_1^2R_z\ln(1-z)$; $z\subset[0,1]$, $R_1=R+\Delta$, and R_z is a geometric parameter, in the present model 100 μm.

Continuity for both temperature and heat flux is required at the boundary. At the bubble wall, the latent heat from the vapor condensation is also considered,

$$T(r,t)|_{r=R}=T_l(r,t)|_{r=R},\qquad \left(q+\dot{m}l+\lambda_l\frac{\partial T_l(r,t)}{\partial r}\right)_{r=R}=0, \tag{10}$$

where l is the latent heat, which can be estimated by interpolating the experimental data. It is found that the latent heat decreases as the temperature increases, and when the temperature gets to or exceeds the critical temperature, $l=0$. At the interface where the two parts partitioned, we have the following conditions:

$$T_l(r,t)|_{r=R_1}=T_l(z,t)|_{z=0},\qquad \left.\frac{\partial T_l(r,t)}{\partial r}\right|_{r=R_1}=\frac{1}{R_z}\left.\frac{\partial T_l(z,t)}{\partial z}\right|_{z=0}, \tag{11}$$

In the far field, the temperature is just the ambient temperature $T_l(z,t)|_{z=1}=T_\infty$. The hydrodynamic equations (4) inside the bubble and the energy equations (7) and (9) in the liquid joining with any MRP equation and the boundary conditions provided can be numerically solved. We find the general differential scheme is appropriate in the computation of the PDE.

E. Bremsstrahlung formulas for SBSL

The electron-atom and electron-ion bremsstrahlung and the recombination radiation are generally considered as the main mechanisms of SBSL. In the present model, this simple bremsstrahlung model is employed to evaluate the light emission. The stimulation of light emission by this simple bremsstrahlung model does not require very high temperature; weakly ionized gases may also produce the sonoluminescence. The estimated maximum temperature of a sonoluminescing bubble is no more than a few decades of thousands of degrees, generally it is $7-30\times10^3$ degrees Kelvin; a gas bubble of ~1 μm radius under these temperatures is optically thin to the bremsstrahlung and the recombination radiation.

The radiation power per wavelength (in micrometers) interval by the electron–neutral-atom bremsstrahlung [20] is, therefore, formulated as

$$\frac{dP_a(t)}{d\lambda}=0.149\,54\int\frac{n_e n_{\text{atom}}\kappa(\lambda,T)}{\{\exp[hc/(\lambda kT)]-1\}\lambda^5}dV, \tag{12}$$

where n_e is the number density of the ionized electron, n_{atom} the number density of the neutral atom, λ the wavelength (in micrometers), h the Planck constant, c the light speed, and κ the free-free atomic absorption coefficient. κ of inert gases can be found in Ref. [20], but there are no data available for water vapor. In the calculation of electron–water-vapor-molecule bremsstrahlung, as an approximation, κ of oxygen is employed instead. In fact, the contribution from this part is relatively minor. The radiation power per wavelength (in micrometers) interval by the electron-ion bremsstrahlung and the recombination radiation together [5] is

$$\frac{dP_i(t)}{d\lambda} = 1.03 \times 10^{-11} hc \int \frac{n_e^2 \exp[hc/(\max(\lambda,\lambda_2)kT)]}{\{\exp[hc/(\lambda kT)] - 1\}\lambda^2 T^{1/2}} dV, \quad (13)$$

where λ_2 is the wavelength corresponding to the first excited energy level of the atom, 0.26 μm for helium, 0.2825 μm for argon, and 0.325 μm for xenon. As an approximation, the λ_2 of water molecule is simply treated to be identical to that of the corresponding inert gas. The spectrum of SBSL can then be calculated as $\int dP(t)/d\lambda\, dt$, while the light pulse shape for a given wavelength is described by $dP(t)/d\lambda$.

The radiation by bremsstrahlung occurs only when ionized free electrons are present. The Saha equation is usually employed to evaluate the number density of the ionized electrons. For a weakly ionized gas mixture, the electron number density can be roughly estimated as

$$n_e = 2\left(\frac{2\pi m_e kT}{h^2}\right)^{3/4} \sqrt{\sum_i n_i \exp[-(\varepsilon_i - \Delta\varepsilon_i)/kT]}, \quad (14)$$

where m_e is the mass of electron, n_i the number density, ε_i the ionization potential, and $\Delta\varepsilon_i$ the reduction of the ionization potential of the ith molecule. The ionization potential of the molecule or atom is usually lowered in a dense gas, and this reduction will be evaluated in the same manner as in Ref. [7].

III. NUMERICAL RESULTS

For numerical computation, some concrete parameters are needed other than those listed in the previous section, such as the specific value of the ambient bubble radius R_0. These parameters may be assigned arbitrarily, but may rather be chosen from some experiments so that the computed results will be more practical. With the consideration above, we shall refer to the experiment conducted by Vazquez and Putterman [21]. In this experiment, single bubbles were generated in water under various conditions and the corresponding emitted light intensities were measured. The ambient temperature of water was varied between 0 and 34 °C and the gas filling the bubble was changed from argon to helium and to xenon. Data with the same ambient radius R_0 and the same maximum radius R_m were obtained in [21] for various ambient water temperatures and filling gases. Many of the concrete parameters employed in this experiment will then be used in our computation below [22].

A. Predicted temperature inside the bubble

The temperature inside an Ar bubble in water is computed, first when the MRPs are varied and next when α is varied. Then the inert gas in the bubble is varied from Ar to Xe or He.

1. Modified Rayleigh-Plesset equations varied for an Ar bubble

Temperatures (and pressures in some cases as well) as functions of time and space inside Ar bubbles for different ambient water temperatures are numerically calculated from the model elements listed in Sec. II. As mentioned in the Introduction, it is our aim to study the effect of using slightly different MRPs and also that of using different accommodation coefficients α. The temperature profiles computed from four different MRPs with $\alpha = 0.4$ and at three ambient temperatures are given in Fig. 1. In Fig. 1 and the following Figs. 2–4, each plot is composed of several curves which are labeled from *a* to *c*, *d*, *e*, or *f*. Curve *a* corresponds to the time when the bubble is compressed to its maximum crushing speed while the last curve (*c*, *d*, *e*, or *f*) corresponds to a time a few tens or hundreds of picoseconds after the rebound. The corresponding radius for each curve can be read directly from the horizontal component of the curve length.

In Fig. 1, the most prominent feature is the appearance of shock waves in the results computed from MRP2 and MRP4 which are just the classical RP equation and its modified version with $\rho_{l\infty}$ and $c_{l\infty}$ replaced by ρ_l and c_l, respectively, and their absence in those computed from the other two MRPs, which are the Keller-Miksis equation and its similarly modified version. In the case of absence of the water vapor, the same trend that the shock formation depends on the form of RP equation was revealed in early studies [23,24].

On examining the plots in Fig. 1 for MRP2 or for MRP4, it will be noticed that the shock wave becomes increasingly stronger when the ambient temperature increases from 0 to 34 °C. Since more water vapor is expected inside the bubble when the ambient temperature is higher, one might infer that the preponderance of water vapor promotes the excitation of a shock wave [25]. This is true for MRP2 and MRP4, but when different MRPs are involved, the content of water vapor does not appear to be a decisive factor. This can be seen in Table I where we computed the amount of water vapor retained in the corresponding bubbles of Fig. 1. The table indicates almost the same β_v, the percent ratio of the number of water vapor molecules to the total number of molecules inside the bubble at its minimum radius, for the four MRPs at the same ambient temperature. In Table I are listed in addition to the computed N_p's for various MRPs at the three ambient temperatures, where N_p is the number of photons emitted per flash by the relevant bubble. In the table, corresponding experimentally observed N_p's in Ref. [21] are also quoted. The disquieting results appearing in Table I are that the emitted photon numbers calculated by the bremsstrahlung model are sensitive to those slightly different MRPs. It may lead to decrease or even loss of the reliability of the calculated results.

From Fig. 1 it will also be noted that the existence of the shock wave does not imply extremely high temperature inside the bubble. This is quite different from earlier deductions when water vapor was absent in the SBSL calculation.

2. The accommodation coefficient varied for an Ar bubble

Figures 2 (for 0 °C) and 3 (for 34 °C), for which MRP4 is used, specify the effect of varying the value of α, the accommodation coefficient. In correspondence with these figures, the β_v's, the % ratios of water vapor, are computed and shown in Table II.

Evidently, the larger the α, the smaller is the amount of water vapor being retained in the compressed bubble. In ad-

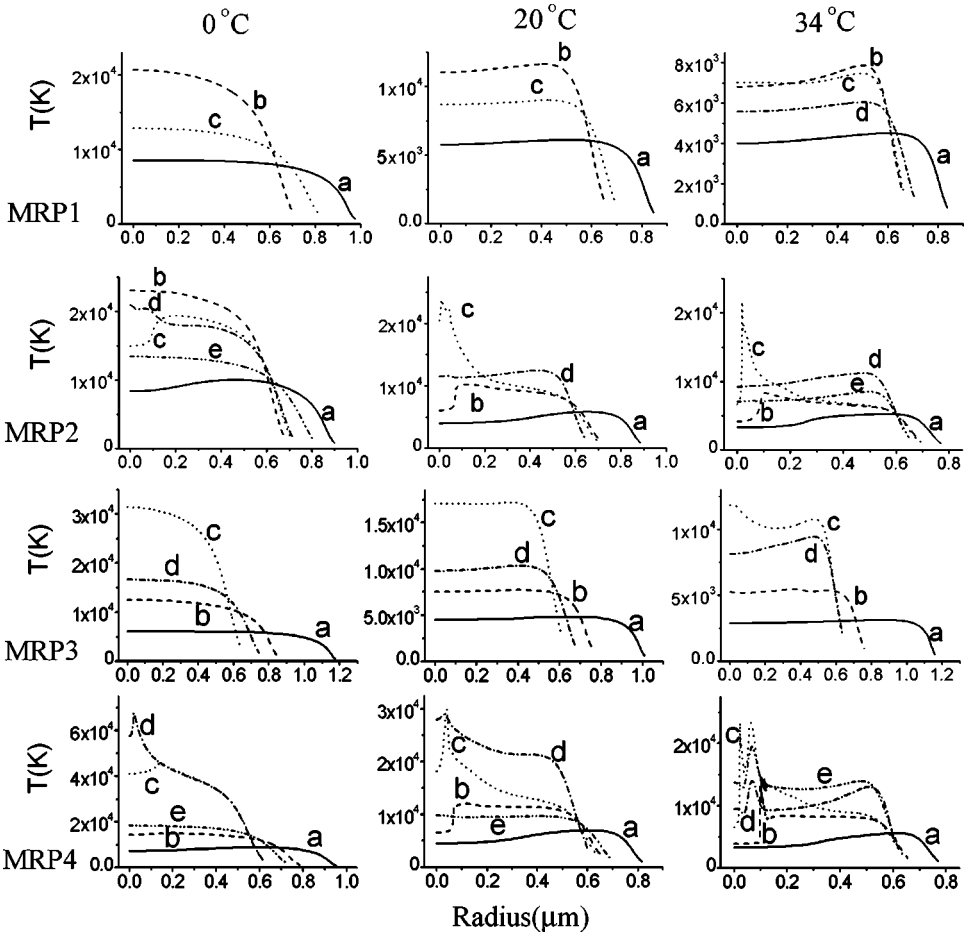

FIG. 1. Spatial profiles and time distribution at the minimum bubble radius of the calculated temperature in an Ar bubble grown in water at $T_\infty=0$, 20, and 34 °C, respectively, as computed from MRP1, MRP2, MRP3, and MRP4 with $\alpha=0.4$, $p_\infty=1$ atm, $R_0=4.55$ μm, and corresponding f and p_a as given in Table I. For the meaning of a–e see text.

dition, we can see that a shock wave appears inside the Ar bubble for $\alpha=0.1$ in Fig. 2 and for both $\alpha=0.4$ and 1.0 in Fig. 3. In Fig. 2, as $\alpha>0.1$ the shock wave disappears; in Fig. 3, the shock wave for $\alpha=0.4$ is stronger than for $\alpha=1.0$. It demonstrates that the larger α would be more propitious for shock formation. Figures 2 and 3 then predict that the larger the α, the higher is the maximum temperature in the bubble, regardless of whether there is shock formation or not. In Table II, the corresponding N_p's are listed once more for later reference.

B. Different inert gas bubbles

In this section, we extend our discussion to two other inert gases (besides Ar) in the bubbles, that is, Xe and He. We shall confine ourselves to the choice of the combination of MRP4, $\alpha=0.4$, and 20 °C to compute the spatial and temporal distributions of temperature and pressure in the bubbles containing these three gases, respectively, under conditions mainly the same as in the previous Figs. 1–3. We find it interesting to compare our computed results with those presented in a recent paper [26]. In that paper, single bubbles of He, Ar, and Xe mixed with water vapor were investigated for the physical state inside the bubbles. The ambient water temperature was room temperature; the other parameters were not exactly the same as assumed in our paper. The authors used the modified Keller equation which is similar to MRP3 (contrary to our MRP4) for the radial motion of the bubble wall and assumed several different amounts of water vapor inside the bubble.

Our computed results are provided in Fig. 4. The figure shows that shock waves are formed in Ar and Xe bubbles but not in the He bubble. For 20 °C and $\alpha=0.4$, we computed the corresponding water vapor content in the compressed bubbles to find $\beta_v=14\%$ in He and 17% in both Ar and Xe. We also computed the maximum speed of the compressed bubble wall to be 3142 m/s for He, 1915 m/s for Ar, and 1149 m/s for Xe. We likewise computed the corresponding number of emitted photons per flash with the results of 4.7×10^4 for He, 5.7×10^4 for Ar, and 1.7×10^5 for Xe. We quote these figures only for reference and shall not attempt to apply them to any physical interpretation of the computed outcomes.

Reference [26] reported the computed result of the occurrence of a shock wave in Xe but not in Ar (a result similar to ours; cf. Fig. 1 above) and He bubbles. It furthermore predicted that the shock wave appeared in Xe only when the water vapor content in the bubble was relatively large, for example, when it was 30%, but could not be the case, for example, when it was 10%. A maximum temperature of the order of 1.1×10^5 K was predicted in the 70% Xe–30% water vapor bubble.

C. Predicted light intensity, pulse, and spectrum

Under the exploitation of Eqs. (12)–(14), the characteristics of the light emitted during the bubble collapse can be

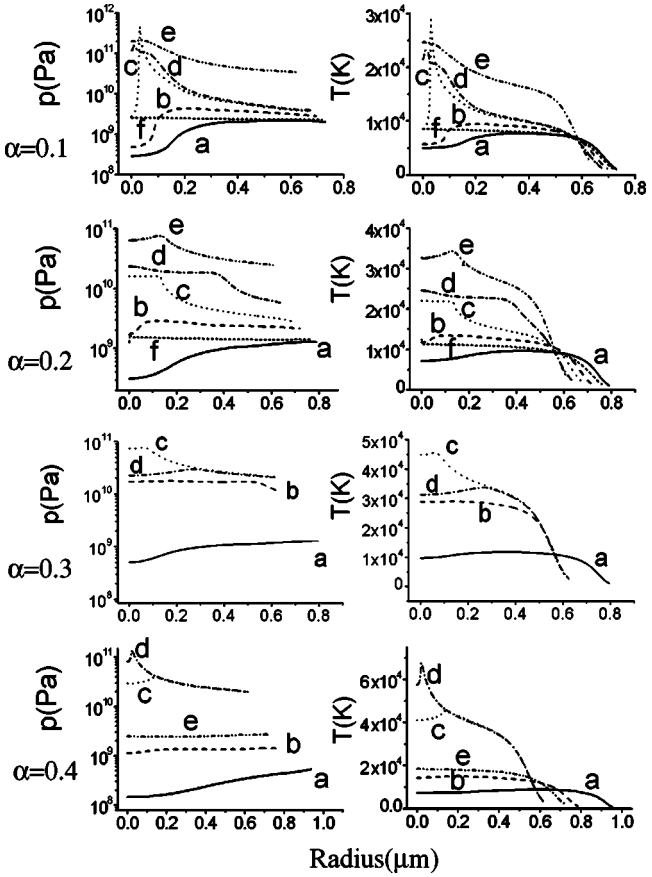

FIG. 2. Spatial profiles and time distribution at the minimum bubble radius of the calculated pressure and temperature in an Ar bubble grown in water at $T_\infty=0$ °C, as computed from MRP4 with various α's and $p_\infty=1$ atm, $R_0=4.55$ μm, and the corresponding f and p_a are given in Table I. The meaning of $a-e$ is the same as in Fig. 1.

calculated. The values will depend on the elements chosen, i.e., in the present case, on the choice of the MRP and the accommodation coefficient.

The computed light intensities in terms of the number of emitted photons per flash, N_p, for the cases considered in Fig.

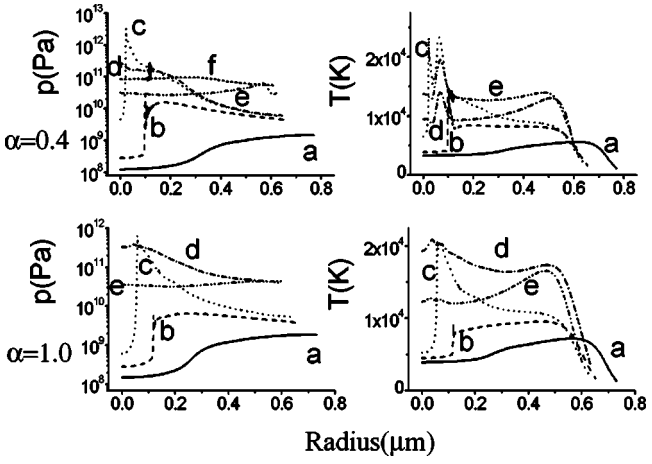

FIG. 3. Same as Fig. 2, but the bubble is in 34 °C water.

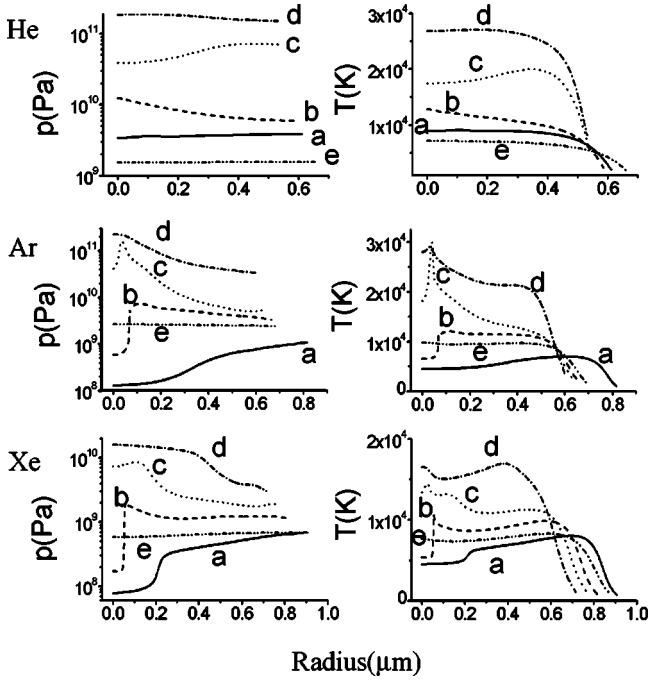

FIG. 4. Spatial profiles of the calculated pressure and temperature of different inert gas bubbles at their minimum radius are calculated by MRP4 for a bubble in 20 °C water and with $\alpha=0.4$ and $p_\infty=1$ atm, $R_0=4.55$ μm, and with the corresponding f and p_a given in Table I. The meaning of $a-e$ is the same as in Fig. 1.

1 for three ambient water temperatures, $\alpha=0.4$, and all MRPs, are listed in Table I. The N_p of an Ar bubble, for the cases considered in Figs. 2–4 for three ambient temperatures, all α's, and MRP4, are listed in Table II. In these two tables, the corresponding N_p experimentally observed in Ref. [21] under similar conditions were also listed, merely for some reference instead of exact comparison, because in this paper accompanying chemical reactions are not taken into account.

From Table I it will be seen that N_p increases rapidly as the ambient temperature decreases. This was thought to be evidence for the presence of water vapor in the bubble, on the basis of the numerical results that the lower the ambient temperature is, the lower the vapor content will be, and consequently the higher the interior temperature will be. Similar results are obtained by the calculation of the uniform pressure approximation [27]. It will also be seen that in Table I, various MRPs provide different N_p's, with the MRP1 delivering the least values and MRP4 the largest. Some N_p's are so small, such as that provided by MRP1 at 34 °C, that barely any light emission can be observed. The situation is expected to worsen if chemical reactions were taken into account. On the other hand, suppose we venture to adopt variable values of α in combination with MRP4, for example, if we adopt $\alpha=0.3$ at 0 °C, $\alpha=0.4$ at 20 °C and $\alpha=1.0$ at 34 °C, with the assumption herein that α is a function of temperature, the computed values of N_p will apparently agree with the experimental values measured in Ref. [21] and quoted in both Tables I and II.

Next, let us address the spectrum of the emitted light. This quantity can be computed from Eqs. (12)–(14). Some computed spectra for argon bubbles at three ambient water tem-

TABLE I. N_p and β_v (in parentheses) at the three ambient water temperatures computed from various MRPs for the single bubbles studied in Fig. 1. In the last row, experimental N_p's in Ref. [21] are quoted.

T_∞ (°C)	0	20	34
f (kHz)	31.9	33.8	34.3
p_a (atm)	1.35	1.34	1.31
N_p (β_v) (MRP1)	3.2×10^4 (5.7%)	3.7×10^2 (18%)	3.3×10^0 (33%)
N_p (β_v) (MRP2)	8.1×10^4 (5.9%)	9.0×10^2 (18%)	1.6×10^2 (34%)
N_p (β_v) (MRP3)	5.2×10^5 (5.2%)	1.3×10^4 (16%)	1.3×10^2 (31%)
N_p (β_v) (MRP4)	2.0×10^6 (5.4%)	5.7×10^4 (17%)	1.2×10^3 (32%)
N_p (expt.)	6.0×10^5	6.0×10^4	1.2×10^4

peratures are provided in Fig. 5, with the same physical parameters R_0, p_∞, f, and p_a as those assumed in Fig. 1 and Table I. Here we use the adjusted α's, for the same reason as discussed in the last paragraph, in order to attempt to obtain more realistic shapes of the spectra. In Fig. 5, individual contributions from different optical mechanisms are shown, including that from the electronic–vapor-molecule bremsstrahlung. It will be seen that the main contribution comes from the electron–inert-gas-atom bremsstrahlung. This is consistent with some earlier findings [3].

The curves of P_λ in Fig. 5 all have dips at $\lambda=0.5$ μm. This is due to the use of linear interpolation of $\kappa(\lambda,T)$ to obtain the values of κ from the values of κ at $\lambda=0$, 0.5, and 1 μm (and various T) which are the only values available to us [20]. It may be noted that $\kappa(\lambda=0.5\ \mu\mathrm{m},T)$ is only known for $T\leqslant2\times10^4$ K but in the present cases, T occasionally exceeds 2×10^4 K (see Figs. 1–4). For the sake of simplicity, the value of $\kappa(\lambda,T)$ at 2×10^4 K is applied to those cases with temperature higher than 2×10^4 K. Hence the value of $\kappa(\lambda,T)$ is underestimated and so is the bubble light emission.

Now we come to the investigation of the light pulse width. For the three cases in Fig. 5, we also obtained the optical pulses of the emitted light, respectively. Figure 6 shows the emitted power vs time for three ambient temperatures. In the figure, the variation with time of the radius of the bubble near the minimum radius is also illustrated. It will be noticed that those calculated the full width at half maximum (FWHM) are of the order of 25–40 ps which are of the right order compared to the experimental values although seemingly somewhat smaller [28]. One may also notice in Fig. 6 that some apparent irregularities appear at the tip of the light pulse in the case of 34 °C. Detailed analysis indicates that this is due to the shock formation in the bubble.

Figure 6 is computed for an argon bubble. Similar curves can be computed for bubbles filled with Xe and He, respectively. Figure 7 presents the normalized optical time pulses of He, Ar, and Xe bubbles in 20 °C water at four different wavelengths, respectively, whereas Fig. 8 indicates the wavelength dependence of their FWHMs. Figures 7 and 8 are, however, based on the results in Fig. 4 in which $\alpha=0.4$ is used instead of the variable α's. From Fig. 8 it can be seen that for He and Ar, the FWHMs are almost wavelength independent as observed [29], whereas for the Xe bubble, the FWHM varies slightly with wavelength, as predicted by Ref. [5].

IV. SUMMARY AND DISCUSSION

We have numerically computed the temperature within and the sonoluminescence characteristics of a stable bubble grown in water and acted upon by an applied acoustic field. The bubble contains one of three inert gases and the water vapor may be at one of three ambient temperatures. The model of computation takes into account the usual physical content or phenomena: the motion of the bubble wall, the motion of the gas mixture inside the bubble, the phase transition of water at the gas-liquid interface, and the variation of temperature of the water surrounding the bubble when the heat transfer at the bubble wall is included. Nevertheless, the physical content of occurrence of the chemical reactions inside the bubble is not within consideration. This neglect will overestimate the temperature inside the bubble and consequently the brightness of the SB. The equations used to describe these physical contents are quoted from well-known

TABLE II. N_p and β_v (in parentheses) for the different α's and three different ambient temperatures calculated by MRP4, with the other parameters the same as in Table I. In the last row, experimental N_p's in Ref. [21] are quoted.

T_∞ (°C)	0	20	34
N_p (β_v) ($\alpha=0.1$)	7.9×10^3(24%)		
N_p (β_v) ($\alpha=0.2$)	3.0×10^5(12%)		
N_p (β_v) ($\alpha=0.3$)	6.6×10^5(7.6%)		
N_p (β_v) ($\alpha=0.4$)	2.0×10^6(5.4%)	5.7×10^4(17%)	1.2×10^3(32%)
N_p (β_v) ($\alpha=1.0$)			9.6×10^3(24%)
N_p (Expt.)	6.0×10^5	6.0×10^4	1.2×10^4

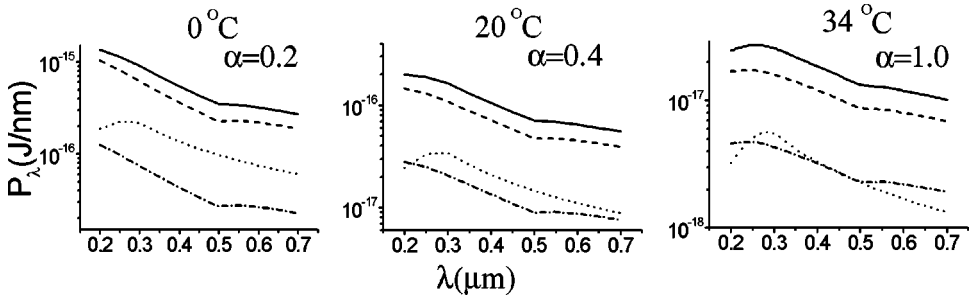

FIG. 5. Computed spectra of argon bubbles at three ambient temperatures (solid line). MRP4 is used for computation and different α's are adopted at different ambient temperatures. Individual contributions from electron-ion bremsstrahlung and recombination radiation combined (dotted line), electron–inert-gas-atom bremsstrahlung (dashed line), and electron–vapor-molecule bremsstrahlung (dash-dotted line) are simultaneously shown.

references. These equations are solved to compute the spatial and temporal distributions of temperature inside the bubble in the neighborhood of its minimum radius. From these values of temperature, the sonoluminescence characteristics, the bubble brightness, the optical spectrum, and the optical pulse width, are computed, by adopting the weak ionization theory and the bremsstrahlung mechanism.

Therefore, the computation seems to be just some incomplete routines, except that we have tried to vary (for illustration) the two equations describing the radial motion of the bubble wall and the evaporation and condensation of the water vapor at the gas-liquid interface, respectively. The former equation is varied by choosing either of its several well-known modified versions. Usually one or other version was used by earlier authors. The latter equation is varied by varying an enclosed parameter which is the accommodation coefficient of water vapor. This coefficient was usually specified at some constant value for some given reason.

Our variation of the individual model elements provides results that differ significantly in some cases. As an example, the temperature reaching in a bubble on the basis of MRP1 with $\alpha=0.4$ is so low that it denies almost any light emission when water temperature is 34 °C (see Table I) whereas the temperature computed from MRP4 with $\alpha=1.0$ better approaches (yet not sufficiently) the experimentally observed value (see Table II). Another case in point, shock waves are predicted to exist in both Xe and Ar bubbles when MRP4 is adopted (Fig. 4), but not in the Ar bubble and only in the Xe bubble when MRP3 is applied (Fig. 1). Reference [26], using the modified Keller equation, which is similar to MRP3, arrived at the same conclusion. Reference [26] offered very apt physical interpretations of the occurrence of a shock wave in the Xe bubble and its absence in the Ar bubble. (We may likewise add to the reasons for the absence of the shock wave in the He bubble the high sound velocity.) Yet the presence of a shock wave in the Ar bubble as predicted in our computation demands additional considerations. Likely the way the bubble is compressed by the liquid should be within the physical interpretation.

The results obtained in the present paper thus point to the importance of choosing not only the proper model "contents," but also the proper (or the most proper) model "element" for each "content" concerned. In the field of stable SBs, it seems to be a rather complicated or difficult problem since a large number of physical elements with their respective varieties exit and some of them concern rather new or incompletely investigated frontiers. We think that more experimental studies on SBs and more comparisons among the various element versions will help to reveal the reality of nature.

ACKNOWLEDGMENTS

This work is supported by NSFC under Grants No. 10174045 and No. 10434070.

APPENDIX A: FORMULAS OF MASS DIFFUSION FLUX HEAT FLUX, AND VISCOSITY

The diffusive mass flux J_1 is provided by the molecular thermal kinetic theory [30]

$$J_1 = -\frac{n^2 M_1 M_2}{\rho} D_{12}\left[\frac{\partial x_1}{\partial r} + \left(x_1 - \frac{\rho_1}{\rho}\right)\frac{\partial}{\partial r}(\ln p) + k_T \frac{\partial}{\partial r}(\ln T)\right], \tag{A1}$$

where n is the number density of the gas mixture, M_i is the molecule mass and x_i the mole fraction of the ith gas, respec-

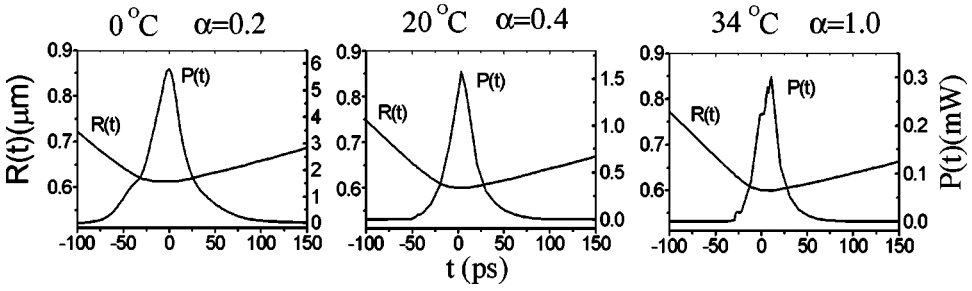

FIG. 6. Emitted optical power $P(t)$ vs time of an Ar bubble computed at three ambient temperatures corresponding to the cases in Fig. 5. The time refers to the time of the bubble radius $R(t)$ being in the neighborhood of the bubble collapse.

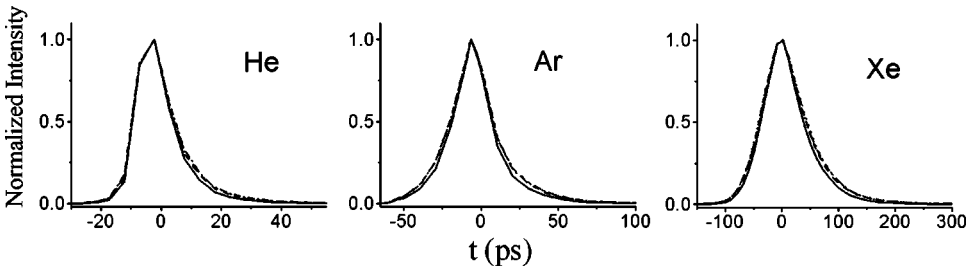

FIG. 7. Optical pulses, normalized to unit height, from bubbles filled with He, Ar, and Xe, respectively, at ambient temperature of 20 °C, computed with $\alpha=0.4$ and MRP4, as in Fig. 4. For each bubble, pulses shown for λ are 250 nm (solid line), 400 nm (dashed line), 550 nm (dotted line), and 700 nm (dash-dotted line), respectively.

tively, D_{12} the binary diffusion coefficient, and k_T the thermal diffusion ratio. For D_{12}, the form provided by Wilke and Lee [18] is employed,

$$D_{12}=\frac{(3.03-0.98/M_{12}^{1/2})(10^{-3})T^{3/2}}{pM_{12}^{1/2}\sigma_{12}^2\Omega_D}, \tag{A2}$$

where $M_{12}=2M_1M_2/(M_1+M_2)$, $\sigma_{12}=(\sigma_1+\sigma_2)/2$ for each component, the characteristic Lennard-Jones length can be evaluated as $\sigma_i=1.18V_{bi}^{1/3}$, V_{bi} is the liquid molar volume, which is estimated as $V_{bi}=0.285V_{ci}^{1.048}$, and V_{ci} is the critical volume of the ith gas. Ω_D is the diffusion collision integral,

$$\Omega_D=\frac{1.060\,35}{(T^*)^{0.1561}}+\frac{0.193}{\exp(0.476\,35T^*)}+\frac{1.035\,87}{\exp(1.529\,96T^*)}+\frac{1.764\,74}{\exp(3.894\,11T^*)}, \tag{A3}$$

where $T^*=kT/\varepsilon_{12}$, $\varepsilon_{12}=\sqrt{\varepsilon_1\varepsilon_2}$, and ε_i is the characteristic Lennard-Jones energy of the ith gas. The thermal diffusion ratio

$$k_T=\frac{105}{118}\frac{M_1-M_2}{M_1+M_2}\frac{59(6C^*-5)(2A^*+5)}{7A^*(55+16A^*-12B^*)},$$

where A^*, B^*, and C^* are functions of T^*, which can be checked from Ref. [30].

The heat flux for two kinds of the gas mixture is [30]

$$q=-\lambda\frac{\partial T}{\partial r}+\left[\frac{\rho}{\rho_1\rho_2}pk_T+\frac{5}{2}kT\left(\frac{1}{M_1}-\frac{1}{M_2}\right)\right]J_1, \tag{A4}$$

where λ is the thermal conductivity. For the low pressure gas mixtures [18],

$$\lambda=\lambda^0=\frac{x_1\lambda_1}{x_1+x_2A_{12}}+\frac{x_2\lambda_2}{x_2+x_1A_{21}}, \tag{A5}$$

where λ_i and x_i are the thermal conductivity and the mole fraction of the ith gas, respectively, and A_{12} and A_{21} are approximately expressed as

$$A_{12}=\frac{[1+(\mu_1/\mu_2)^{1/2}(M_2/M_1)^{1/4}]^2}{[8(1+M_1/M_2)]^{1/2}},$$

$$A_{21}=A_{12}\frac{\mu_2}{\mu_1}\frac{M_1}{M_2}, \tag{A6}$$

where μ_i is the viscosity of the ith gas. For a good fit to the experimental data [31] $\lambda_i=g_iT^{h_i}$ and $\mu_i=s_iT^{f_i}$, the extrapolation of both expressions to the high temperature case is subjectively assumed to be correct in the present model. Values of the parameters g_i, h_i, s_i, and f_i of some gases are listed in Table III.

The approximate analytical expressions for the high pressure correction of the thermal conductivity [18] are established as

$$(\lambda-\lambda^0)\Gamma Z_{mc}^5=\begin{cases}1.22\times10^{-2}[\exp(0.535\rho_r)-1], & \rho_r<0.5,\\ 1.14\times10^{-2}[\exp(0.67\rho_r)-1.069], & 0.5<\rho_r<2.0,\\ 2.60\times10^{-2}[\exp(1.155\rho_r)+2.016], & 2.0<\rho_r<2.8,\end{cases} \tag{A7}$$

where Z_{mc} is the critical compressibility. For the gas mixture $Z_{mc}=0.291-0.08(x_1\omega_1+x_2\omega_2)$, where ω_i is the acentric factor of the ith gas. The reduced density $\rho_r=\rho_m/\rho_{cm}$, where $\rho_m=x_1\rho_1+x_2\rho_2$, $\rho_{cm}=M_m/V_{cm}$, $V_{cm}=x_1^2V_{c1}+2x_1x_2V_{c12}+x_2^2V_{c2}$, V_{ci} is the critical volume of the ith gas, and $V_{c12}=[(V_{c1}^{1/3}+V_{c2}^{1/3})/2]^3$. $M_m=x_1M_1+x_2M_2$, $\Gamma=210(T_{mc}M_m^3/P_{mc}^4)^{1/6}$, where $T_{cm}=x_1^2V_{c1}T_{c1}+2x_1x_2V_{c12}T_{c12}+x_2^2V_{c2}T_{c2}$, T_{ci} is the critical temperature of the ith gas, and $T_{c12}=\sqrt{T_{c1}T_{c2}}$, $P_{cm}=Z_{cm}\tilde{R}T_{cm}/V_{cm}$.

The viscosity of the high pressure correction is provided by Reichenberg, see Ref. [18],

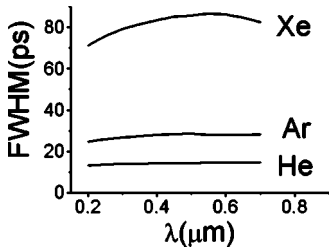

FIG. 8. Wavelength dependence of FWHMs from bubbles filled with He, Ar, and Xe. Conditions are the same as in Fig. 7.

$$\frac{\mu_i}{\mu_i^0} = 1 + Q_i \frac{A_i P_{ri}^{3/2}}{B_i P_{ri} + (1 + C_i P_{ri}^{D_i})^{-1}}, \tag{A8}$$

where $\mu_i^0 = s_i T^{f_i}$, $P_{ri} = x_i p / P_{ci}$ is the reduced pressure, $Q_i = 1 - 5.655 d_{ri}$, d_{ri} is the reduced dipole moment of the molecule, $d_{ri} = 52.46 d_i^2 P_{ci} / T_{ci}$, d_i is the dipole moment in debyes and P_{ci} is the critical pressure of the ith molecule. The constants A_i, B_i, C_i, and D_i are functions of the reduced temperature $T_{ri} = T / T_{ci}$, $A_i = 1.9824 \times 10^{-3} / T_{ri} \exp(5.2683 T_{ri}^{-0.5767})$, $B_i = A_i (1.6552 T_{ri} - 1.2760)$, $C_i = 0.1319 / T_{ri} \exp(3.7035 T_{ri}^{-79.8678})$, $D_i = 2.9496 / T_{ri} \exp \times (2.9190 T_{ri}^{-16.6169})$. For a binary gas mixture of 1 and 2, the viscosity is

$$\mu = K_1 (1 + H_{12}^2 K_2^2) + K_2 (1 + 2 H_{12} K_1 + H_{12}^2 K_1^2), \tag{A9}$$

where

$$K_1 = \frac{x_1 \mu_1}{x_1 + \mu_1 x_2 H_{12} (3 + 2 M_2 / M_1)},$$

$$K_2 = \frac{x_2 \mu_2}{x_2 + \mu_2 x_1 H_{12} (3 + 2 M_1 / M_2)},$$

$$H_{12} = \frac{(M_1 M_2 / 32)^{1/2}}{(M_1 + M_2)^{3/2}} (C_1 + C_2)^2 U_{12},$$

TABLE III. Fitted parameters of viscosity and thermal conductivity of gases.

	g	h	s	f
He	0.003 27	0.678 91	$0.422\,35 \times 10^{-7}$	0.677 42
Ar	0.000 21	0.840 51	$2.15\,99 \times 10^{-7}$	0.777 29
Xe	0.000 03	0.935 49	$1.103\,9 \times 10^{-7}$	0.937 24
H_2O	8.466×10^{-6}	1.346 67	$1.633\,4 \times 10^{-8}$	1.121 38

$$T_{r12} = \frac{T}{(T_{c1} T_{c2})^{1/2}}, \quad d_{r12} = (d_{r1} d_{r2})^{1/2},$$

$$C_i = \frac{M_i^{1/4}}{\mu_i U_{ii}},$$

$$U_{ij} = \frac{[1 + 0.36 T_{rij} (T_{rij} - 1)]^{1/6}}{T_{rij}^{1/2}} \frac{T_{rij}^{3.5} + 10^7 d_{rij}^7}{T_{rij}^{3.5} (1 + 10^7 d_{rij}^7)},$$

$$T_{rii} = T_{ri}, \quad d_{rii} = d_{ri}.$$

APPENDIX B: FORMULAS OF THE VAN DER WAALS CONSTANTS *a* AND *b*

For two kinds of gas mixture, the parameters a and b are taken to vary in the following manner with composition [32]:

$$a = a_{11} x_1^2 + 2 a_{12} x_1 x_2 + a_{22} x_2^2,$$

$$b = b_{11} x_1^2 + 2 b_{12} x_1 x_2 + b_{22} x_2^2. \tag{B1}$$

The constants a_{ii} and b_{ii} are just the constants for the pure components; a_{12} and b_{12} may be estimated roughly as

$$\sqrt[3]{b_{12}} = \frac{1}{2} (\sqrt[3]{b_{11}} + \sqrt[3]{b_{22}}),$$

$$a_{12} = \sqrt{a_{11} a_{22}}. \tag{B2}$$

[1] D. F. Gaitan, L. A. Crum, C. C. Church, and R. Roy, J. Acoust. Soc. Am. **91**, 3166 (1992).
[2] B. P. Barber and S. J. Putterman, Nature (London) **352**, 318 (1991).
[3] L. Frommhold, Phys. Rev. E **58**, 1899 (1998).
[4] K. Yasui, Phys. Rev. E **60**, 1754 (1999).
[5] S. Hilgenfeldt, S. Grossmann, and D. Lohse, Nature (London) **398**, 402 (1999).
[6] C. Camara, S. Putterman, and E. Kirilov, Phys. Rev. Lett. **92**, 124301 (2004).
[7] D. Hammer and L. Frommhold, Phys. Rev. E **65**, 046309 (2002).
[8] B. D. Storey and A. J. Szeri, Proc. R. Soc. London, Ser. A **456**, 1685 (2000).
[9] L. Rayleigh, Philos. Mag. **34**, 94 (1917); M. Plesset, J. Appl. Mech. **16**, 277 (1949); B. Noltingk and E. Neppiras, Proc. Phys. Soc. London, Sect. B **63**, 674 (1950); J. B. Keller and I. I. Kolodner, J. Appl. Phys. **27**, 1152 (1956).
[10] B. P. Barber *et al.*, Phys. Rep. **281**, 65 (1997).
[11] F. R. Gilmore, Caltech Hydrodynamics Laboratory Report No. 26-4, 1950 (unpublished).
[12] A. Prosperetti and A. Lezzi, J. Fluid Mech. **168**, 457 (1986).
[13] J. B. Keller and M. Miksis, J. Acoust. Soc. Am. **68**, 628 (1980).
[14] V. P. Carey, *Liquid-Vapor Phase Change Phenomena* Hemisphere Washington, D.C., 1992).
[15] K. Yasui, Phys. Rev. E **56**, 6750 (1997).
[16] D. Lohse, M. P. Brenner, T. F. Dupont, S. Hilgenfeldt, and B. Johnston, Phys. Rev. Lett. **78**, 1359 (1997).
[17] V. Q. Vuong and A. J. Szeri, Phys. Fluids **8**, 2354 (1996).

[18] R. C. Reid, J. M. Prausnitz, and B. E. Poling, *The Properties of Gases and Liquids*, 4th ed. (McGraw-Hill, New York, 1987).
[19] C. E. Grosh and S. A. Orszag, J. Comput. Phys. **25**, 273 (1977).
[20] S. Geltman, J. Quant. Spectrosc. Radiat. Transf. **13**, 601 (1973).
[21] G. E. Vazquez and S. J. Putterman, Phys. Rev. Lett. **85**, 3037 (2000).
[22] It might be of some interest to note that, in Ref. [21], R_0 was defined as the radius when the pressure inside the bubble was the ambient pressure p_∞ of 1 atm. An alternative is to define R_0 as the radius when the internal pressure is $p_\infty + p_{sf}$ where p_{sf} is the pressure from the surface tension. Accordingly, $R_0 = 5$ μm in Ref. [21] is corresponding to $R_0 = 4.55$ μm in the present paper. A consequence of this slight change in R_0 is an accompanying change in the given amplitude of the driving acoustic pressure, which is to be determined from the observed bubble dynamics curve.
[23] L. Yuan, H. Y. Cheng, M. C. Chu, and P. T. Leung, Phys. Rev. E **57**, 4265 (1998).
[24] C. F. Ying and Y. An, Sci. China, Ser. A: Math., Phys., Astron. **45**, 926 (2002).
[25] W. C. Moss *et al.*, Phys. Rev. E **59**, 2986 (1999).
[26] N. Xu, R. E. Apfel, A. Khong, X. Hu, and L. Wang, Phys. Rev. E **68**, 016309 (2003).
[27] Y. An, C. G. Xie, and C. F. Ying, Chin. Phys. Lett. **20**, 575 (2003).
[28] R. A. Hiller, S. J. Putterman, and K. R. Weninger, Phys. Rev. Lett. **80**, 1090 (1998).
[29] B. Gompf, R. Gunther, G. Nick, R. Pecha, and W. Eisenmenger, Phys. Rev. Lett. **79**, 1405 (1997).
[30] C. T. Ying, *Transport Theory of Gases and Its Application* (Tsinghua, Beijing, 1990).
[31] *Handbook of Chemistry and Physics*, 84th ed., edited by D. R. Lide, (CRC, Boca Raton, FL, 2003–2004).
[32] J. O. Hirschfelder, C. F. Curtiss, and R. B. Bird, *Molecular Theory of Gases and Liquids* (John Wiley & Sons, New York, 1964).